A review of recent experiments on W and high Z materials as plasma-facing components in magnetic fusion devices

Nobuaki Noda [a,*], Volker Philipps [b], Rudolf Neu [c]

[a] National Institute for Fusion Science, Furo-cho, Chikusa-ku, Nagoya 464-01, Japan
[b] Institut für Plasmaphysik, KFA Jülich GmbH, D-52425 Jülich, Germany
[c] Max-Planck Institut für Plasmaphysik, D-85748 Garching, Germany

Abstract

Since the 10th PSI conference in 1992, high Z refractory metals have been attracting growing interest as candidates for plasma facing materials, because of their resistance against erosion. In tokamaks such as TEXTOR, ASDEX Upgrade, FTU, Alcator C-Mod, D III-D, considerable effort has been made to study the behavior of high Z impurity in the core and edge plasmas, erosion/re-deposition processes at the limiter/divertor surfaces, hydrogen isotope retention, material development and tests, etc. An interim review of these studies is given. Tentative conclusions are drawn in order to get a view and direction in the future studies.

Keywords: High Z wall material; Impurity transport; Erosion and particle deposition; Impurity source; Tritium inventory

1. Introduction

For the last two decades, the major emphasis in fusion research has been laid upon demonstration of high temperature plasmas relevant to reactor, even if it would be limited to a few seconds. Wall materials have been chosen always from a viewpoint toward improving plasma core performance, which has led us to the adoption of low Z walls. Now we are facing the next major step of fusion research, in which new criteria should be seriously considered for the material selection, namely: (1) compatibility with long time sustaining of high temperature plasmas, and (2) with an environment of DT-neutron irradiation. Based on this idea, reconsideration of plasma facing materials was proposed in the Monterey Conference in 1992 with inclusion of high Z refractory metals [1], which are attractive because of their erosion-resistance. Since then, considerable efforts have been made in tokamaks to improve the understanding of core plasma and plasma surface interaction (PSI) issues of high Z metals.

Since 1994, the ITER team has been considering adoption of tungsten into some parts (the wings, the dome, and the lower part of the baffle) around its divertor regions [2]. Then the needs for a tungsten database have come to be more urgent.

Since the beginning of the 1980s, tungsten and molybdenum have been less frequently used in fusion plasma experiments because of problems due to radiation loss found in several tokamaks such as PLT [3,4], JT-60 [5], etc. Before that time, edge diagnostics had not been well established. The combination of these two situations results in lack of detail and systematic data on the performance of high Z plasma facing materials (PFM) in plasma devices, especially in tokamaks.

In this paper, an interim review of these studies after 1992 is given, with an emphasis on the impacts of high Z impurities upon core plasmas, their transport in core and edge plasmas, erosion/deposition at surfaces of plasma facing components (PFC), etc.

Material development is another big issue to be explored from now on. Because of a limited space, only a brief introduction is given in this paper on activities and ideas in this field.

It should be emphasized that one of the targets in the final goal of this study is not a simple question to be

* Corresponding author. Fax: +81-572 57 5600; e-mail: noda@nifs.ac.jp.

answered as 'yes' or 'no', but 'in which condition a high Z PFC is available without any serious degradation of core plasma performance, and with a reasonable lifetime'.

2. Impact and behavior of high Z impurities in core plasmas

2.1. Transport of high Z impurities

It is clear that too many high Z impurities at the plasma center causes a destructive impact on plasma behavior due to radiation loss. Actually it was observed that the electron temperature collapse happened due to strong centrally-peaked radiation from tungsten ions in PLT [3]. The questions are: (1) what is the critical density of high Z impurities or density product $n_e n_{imp}$?, (2) how it can be quantitatively decided or explained?, (3) what causes impurity density to build up to the critical value?, (4) how core plasmas behave above the critical density?, etc. It should be mentioned here that the contribution of high Z impurities to Z_{eff} could not be significant at the critical density determined by the radiation loss. Very rough and vague ideas have been given as an answer to these questions of (1)–(4) before a few years ago. For instance, 'an edge temperature below 50 eV is necessary to accept tungsten as the material of the divertor target plates'. However, just a few experiences have been reported on high Z metals including tungsten before 1992. Intensive studies on the core-plasma issues have been started in TEXTOR, ASDEX Upgrade, Alcator C-Mod, FTU, and D III-D since 1992.

It is worthwhile to know more in detail what happens with an excess contamination of high Z impurities, because we need a more exact understanding of the critical condition of the contamination for different materials, such as Mo, Ta, W. The critical condition (which was seen in PLT, etc.) has been reproduced in TEXTOR in 1992 with a small test limiter made of molybdenum [6]. In this experiment, a small test limiter was inserted from 10 to 20 mm inside the last closed surface (LCFS), which was determined by a toroidal belt limiter named ALT-II. Fig. 1 shows the time behavior of plasma parameters with the molybdenum limiter. In Ohmically heated (OH) discharges with a central line-averaged density of 3×10^{19} m^{-3}, a steep increase in central bolometric radiation P_{bol} was observed at 0.8 s in Fig. 1 and the central electron temperature T_{e0} began to decrease at 1.0 s. The electron temperature profile at the central region was flattened toward the time of the maximum radiation, and the profile of the bolometric radiation (P_{bol}) became strongly peaked as shown in Fig. 2. This is usually followed by an oscillatory behavior of the parameters with minor disruptions (see Fig. 1). Quite the same behavior was observed with a tungsten limiter in TEXTOR [7]. It is important that the temperature drop combined with a peaked radiation profile can be seen
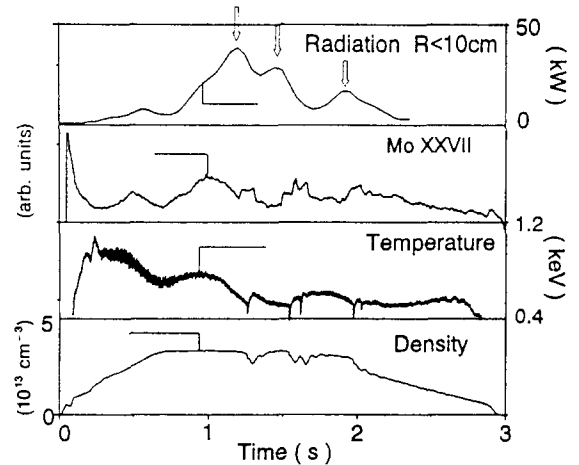

Fig. 1. A critical condition in an Ohmically heated discharge in TEXTOR with a molybdenum test limiter [6]. Time behavior of radiation from plasma center ($r < 10$ cm), brightness of Mo XXVII, central electron temperature, and central line-averaged density are shown. The plasma became unstable after 0.8 s.
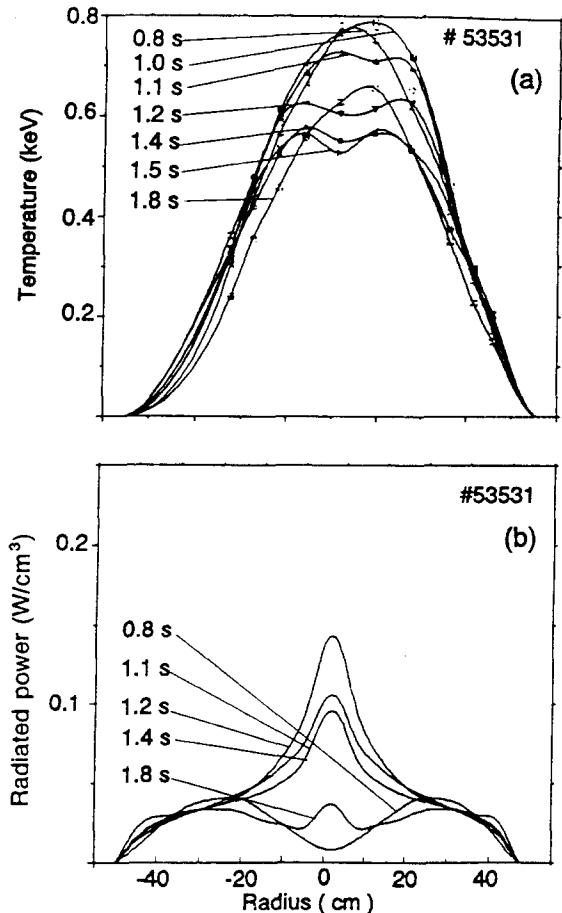

Fig. 2. Electron temperature (a) and bolometric radiation (b) profiles at different times before, during and after the instability shown in Fig. 1 [6].

in only limited cases such as OH operation with a density higher than a critical value [8]. Fig. 3 shows the radial profiles of P_{bol} for NB heated (1.3 MW) discharges with the Mo limiter inside the LCFS [6]. The profiles are hollow, having no peak at the axis. No significant difference can be seen between profiles with limiter in and out for higher line-averaged densities.

In ASDEX Upgrade, strong radiation on axis has been reported not during OH but occasionally in NB heated H mode discharges in a W laser blow-off experiment [8–11]. Fig. 4 shows the time behavior of the parameters. In Fig. 4(c), strong central radiation continues for longer than 0.3 s and the central temperature decreases in this period. It is clear from the figure that the electron temperature profile
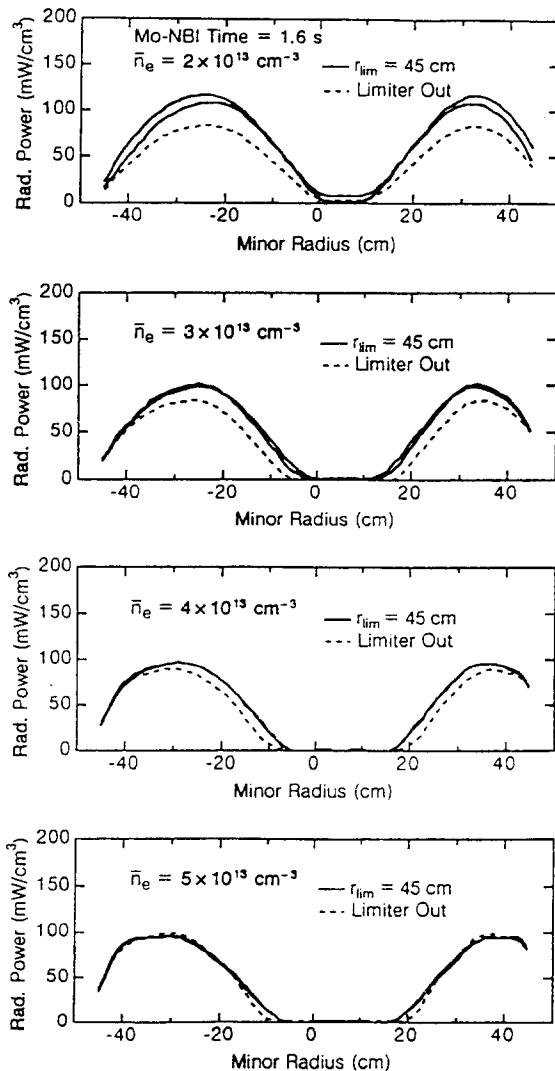

Fig. 3. Radiation profiles with the Mo limiter inserted (solid lines $r = 45$ cm, 1.0 cm inside the last closed flux surface), and withdrawn (dashed lines) for NB heated discharges [6].

became flat after 3.2 s. Oscillatory behavior is not seen in this case. This type of strong radiation loss has not been observed in wide operation range but only in limited cases.

For OH discharges in FTU with a poloidal tungsten limiter, another critical behavior is reported [12–14], that is a hollow electron temperature profile which appears at the start-up of a discharge with a high current (I_p)/density (n_e) ratio. This has been avoided by operating with relatively low I_p/n_e conditions (see Fig. 5).

Different from TEXTOR, no critical density has been observed in FTU. It is probably due to higher I_p with higher B_t, therefore higher OH power input at the plasma axis. This situation is common in Alcator C-Mod, too.

In general, three possible mechanisms should be considered being responsible for the strong and unstable radiation enhancement shown in Figs. 1 and 2. The first is the accumulation of Mo or W ions toward the plasma axis, the second the temperature dependence of radiation power and the third is the increase in external source. The third mechanism can be easily excluded both in TEXTOR and ASDEX cases. Higher density results in lower edge temperature and the sputtered flux always decreases with the edge temperature, which will be shown later (Sections 3.1 and 3.2, Figs. 10 and 11). The source rate is determined by the target and the laser power in laser blow-off experiments. Moreover, as is explained below, the second is judged to be not responsible for the enhanced radiation within the present knowledge.

A discussion on the thermal instability (Fig. 1) in TEXTOR is given by Tokar et al. in an invited paper of the 22nd EPS conference [15]. As seen in Fig. 1, T_{e0} is around 0.8 keV when the radiation starts to rise. According to the calculation by Post and Jensen [16,17], radiation power from Mo is not strongly dependent on T_e around this range in temperature, so the radiation increase is not attributed to a decrease in T_{e0}. There remains a possibility that the region with a strong T_e dependence could be shifted to the lower T_e side compared to the Post–Jensen curves as is discussed later in Section 2.3. But if we would assume the temperature dependence in Refs. [16,17], we could conclude that impurity transport close to the plasma axis is responsible for the radiation increase. The impurity flux density consists of anomalous diffusion and neo-classical convection. The latter has two components, namely an inward flux due to the density gradient and an outward one due to the temperature gradient. At a critical density, the loss by radiation exceeds the ohmic input, which causes a slight decrease in T_{e0}. It initiates a flattening of the T_e profile, namely smaller gradient T_e, which reduces the outward neo-classical convection proportional to the gradient T_e. Then the inward convection exceeds the outward one and the diffusion flux, which causes accumulation of the impurities toward the axis. This is the basic idea given in the literature [15] by Tokar et al. In this argument, it is important that the ions are in the Pfirsch–Schlüter regime. They discussed this process a little more
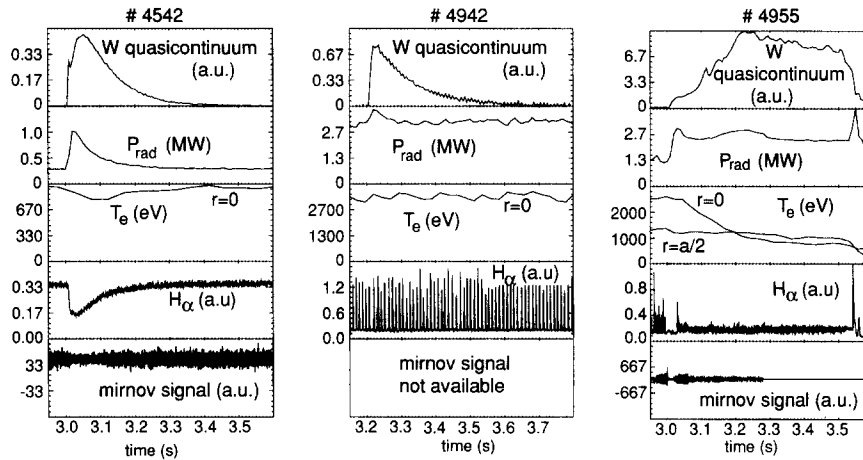
Fig. 4. Time behavior of quasi-continuum from W ions, total radiation P_{rad}, central electron temperature T_e, H α and magnetic fluctuations for an OH discharge (a), for an NB + ICRF-heated H-mode discharge without W accumulation (b), and for an NB-heated discharge with W accumulation (c) in ASDEX Upgrade [10]. Horizontal axis is time in seconds. The total radiation is contributed not only by central radiation but also by radiation from the periphery. Then the higher P_{rad}, does not necessarily resulted in the lowering in the central T_e.

quantitatively and derive the critical plasma density as a function of the ratio of the anomalous to neo-classical diffusion constant and the central impurity density. Further, and clearer experimental evidence for the critical density has been shown in Ref. [8] by Philipps et al. with a tungsten test limiter. Progress in the analyses following the approach given here is expected to give us a more exact, quantitative view on the critical density at the plasma axis.

In addition to the OH case discussed above, there are lots of experimental facts which indicate that transport in the core is playing an important role. In ASDEX Upgrade, no accumulation has been observed in OH discharges (Fig. 4(a)). Another example of an NB (4.6 MW) plus ICRF

(0.9 MW) heated H-mode discharge is shown in Fig. 4(b). Tungsten is injected to the plasma by laser-blow-off at 3.2 s. Quasi-continuum radiation from W decays quickly with an e-folding time of 130 ms, which indicates no accumulation of tungsten even in this H-mode discharge. On the other hand, as is noted previously, the tungsten radiation does not decay for a long time and the central temperature decreases strongly in the case of Fig. 4(c). The difference between these two cases is attributed to a difference in transport. It is pointed out that sometimes the tungsten does not accumulate axisymmetrically. The accumulation happens in a helical structure of such an $m/n = 1/1$ mode close to the plasma axis, which rotates with about 10 kHz
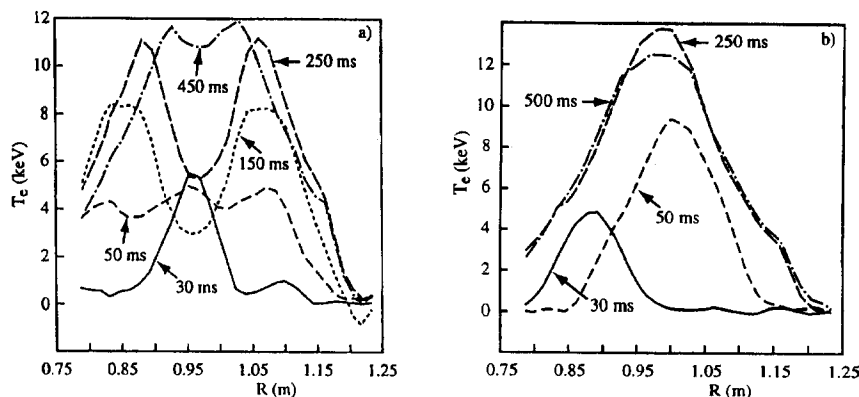

Fig. 5. Electron temperature profiles in ohmic discharges in FTU (a) with high I_p/n_e ratio in startup and (b) with low I_p/n_e [12].
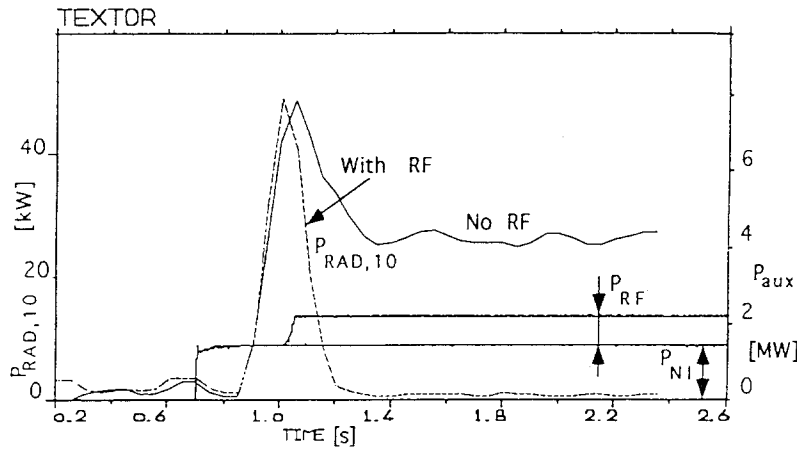
Fig. 6. Reduction of the central radiation by addition of ICRF-heating to NBI in TEXTOR [18].

in the toroidal direction [9–11]. The radial transport of tungsten ions in ASDEX Upgrade is discussed by Naujoks et al. in Ref. [9].

Another example of TEXTOR with a tungsten limiter is given in Ref. [18], where the addition of ICRF heating to an NB heated discharge greatly reduced the central radiation loss (see Fig. 6). The difference in electron temperature is not large with and without ICRF heating. It is also shown that the ICRF heating added to OH discharges reduces the radiation loss [19,20]. In these papers, the authors claim that heating by ICRF with a sufficient power has some impact on impurity accumulation being dissolved, and that there is a certain threshold power of ICRF necessary to realize it. The threshold power level can be interpreted in terms of critical density [15]. It is worth noting that there is no accumulation in Fig. 4(b) in ASDEX Upgrade coincidentally with ICRF heating. In the previous review [1], special attention was given to the ICRF heating with a concern about the enhanced source rate in the plasma edge. Recent experiments have shown that the ICRF gives us a rather favorable effect on high Z impurity behavior by changing transport in the core. The real reason of this 'ICRF effect' is not clear at the moment. It might not be a direct effect of traveling rf waves coupling with impurity ions in the core, but a change in the density and/or temperature profiles or a change in sawtooth activity due to the rf heating triggering the change in transport. Transport issues with additional heating should be more systematically investigated in the future.

In FTU, molybdenum and tungsten concentration in the plasma core has been compared to the influx of these impurities from the limiter during OH discharges. The results suggest that no accumulation in the plasma center occurs within the operation range, at least in standard sawtoothing discharges [12–14]. In Alcator C-Mod, the transport has been investigated with impurity injection by the laser blow-off technique. No big difference in the diffusion coefficient D and inward velocity v_{in} has been

observed up to now in wide range of operations including OH and ICR heating [21,22]. In spite of the full toroidal Mo divertor, no serious influence of radiation loss has been found both in OH and ICRF heated plasmas [23,24]. [1] No accumulation of Mo in the core has been seen during a LH-heated 1 h and 2 h steady state discharges in TRIAM-1M with Mo limiter operation [25].

As a summary, strong accumulation of high Z impurities occurs only in a limited cases in tokamaks, and a wide operation area could be expected.

Another transport problem relating to low Z impurity injection will be discussed in Section 3.4.

2.2. Atomic processes of multiple charged ions

Another big issue in the core concerns atomic processes of highly charged ions. A systematic and comprehensive study on this issue is going on in Alcator C-Mod. In this tokamak, all the tiles in the divertor and the inboard wall are made of molybdenum [23]. Radiation profiles from multiple-charged molybdenum ions have been precisely investigated. A five chord, spatially scannable crystal spectrometer array is used to analyze line emissions from Mo^{31+}–Mo^{33+} in the range of 2.8 to 4.1 Å [21,26,27]. Another spatially resolved VUV spectrometer has been dedicated to measure radiation from Mo^{23+}–Mo^{31+}. Symbols in Fig. 7 show measured brightness profiles with 1 MW ICRF heating. In order to reproduce the brightness profile, the following analysis has been made.
1. Charge state distribution is calculated from the MIST [28] impurity transport code.

2. Measured profiles are used for input data of electron density and temperature.
3. Diffusion constant and inward velocity are deduced from laser blow-off experiments.
4. Fractional abundance of molybdenum charge states are calculated using ionization and recombination rates.
5. Excitation rates used to calculate emmissivity and brightness profiles are of individual lines.

In Fig. 8, two sets of the fractional abundance are shown obtained through procedures (1)–(4). The results in Fig. 8(a) is obtained using the new ionization and recombination rates, in which 'excitation auto-ionization (EA)' is taken into account [29]. Those in Fig. 8(b) are obtained using older ionization and recombination rates without EA and with a semi-empirical form for dielectronic recombination (DR). A marked difference can be seen in the abundance of Mo^{32+} and Mo^{33+} between the results of Fig.
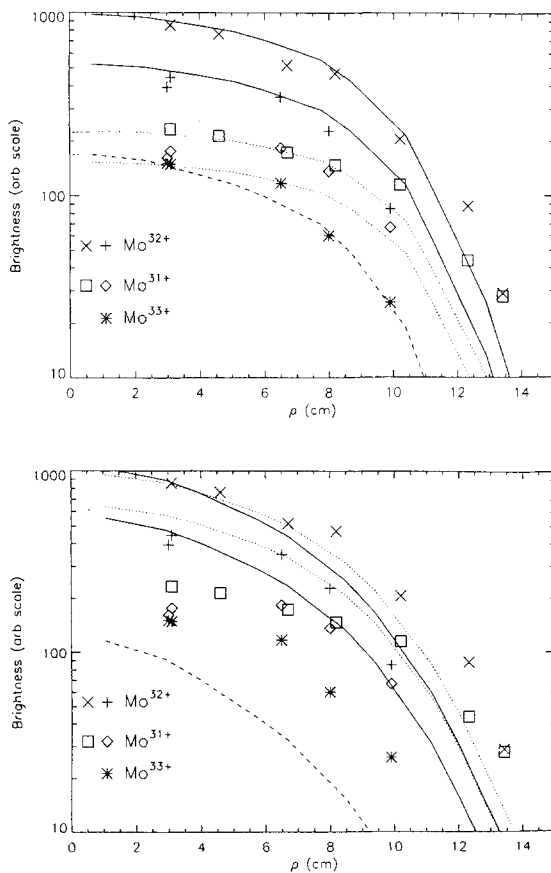

Fig. 7. Measured (symbols) and calculated (lines) X-ray brightness profiles (the horizontal axis ρ indicates the minor radius). The solid lines are from Ne-like molybdenum, dotted line from Na-like, and dashed line from F-like. Measured data are obtained during ICRF heating in Alcator C-Mod. The calculation was done based on charge state density profiles shown in Fig. 8, obtained (a) with excitation auto-ionization (EA) and new dielectronic recombination (DR) rates, and (b) without EA and with old DR rates [21].
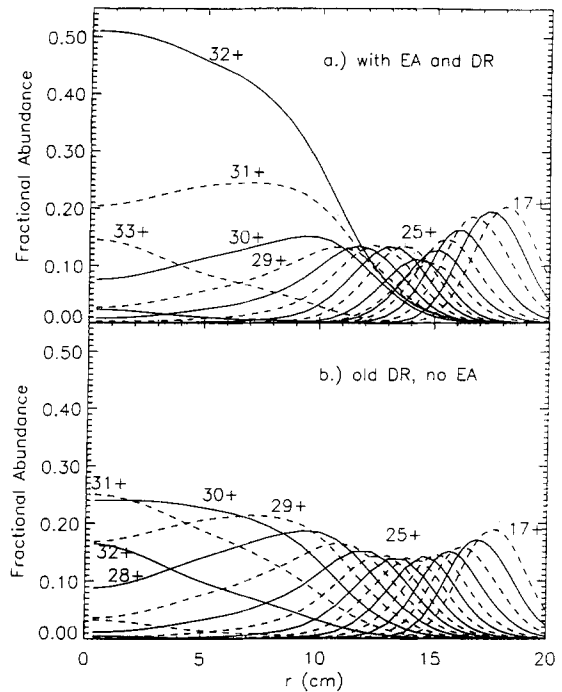

Fig. 8. Calculated molybdenum charge state radial profiles, (a) with the EA processes and new DR rates, (b) without the EA processes and old DR rates. Solid lines are even charge state and dashed lines are for odd ones [21].

8(a) and (b). Ions reach higher charge states because of the larger ionization rate due to the additional process of the EA. Lines in Fig. 7(a) and (b) are plots of the chord brightness obtained with the charge state profiles in Fig. 8(a) and (b), respectively, by using the same excitation rates. It is seen that the measured profile agrees well with the calculated results in Fig. 7(a), where the profile of Mo^{32+} and Mo^{33+} in Fig. 8(a) gives a significant contribution. On the other hand, deviations of calculated profiles are seen in Fig. 8(b) where the EA process is not taken into account. This indicates the importance of the EA process for the calculation of the fractional abundances of highly charged Mo ions. The EA process could be also important in highly charged tungsten ions. Experimental results and calculated approach similar to the one described above are near term issues to be explored.

Spectroscopic studies for tungsten ions are also in progress in ASDEX Upgrade [9–11]. Ionization stages with charge number of up to 50 have been identified in NB heated discharges. Some single lines were identified as those of Br- and Cu-like tungsten ions as is shown in Fig. 9.

2.3. Cooling rates by high Z impurity radiation

In TEXTOR and ASDEX Upgrade, the Mo or W ion densities are estimated from the measured bolometric radi-
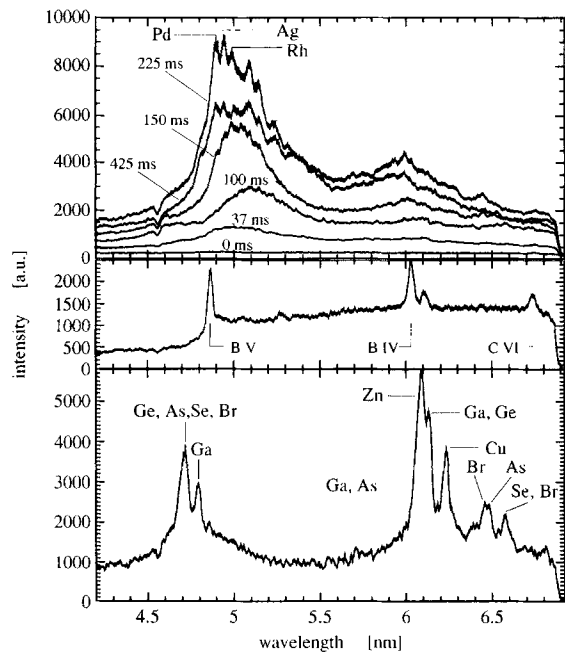
Fig. 9. Integral intensity of the W transition array before and after laser blow-off into ASDEX Upgrade: (top) tungsten radiation spectra for a discharge in which strong tungsten accumulation to the plasma axis occurs ($T_e = 1$ keV), times in the figure are measured from the time of W injection, (middle) the same wavelength region before laser blow-off in an H-mode discharge, (bottom) with additional single tungsten lines in an NB heated H-mode discharge ($T_e = 2$ keV) [10]. The element symbols are iso-electronic sequences of the W lines.

ation intensities using the Post–Jensen cooling curves [16,17]. As mentioned already in Section 2.1, radiation enhancement of molybdenum impurity ions is discussed based on this calculation, too. The target value of the impurity density has been estimated usually from these curves in discussions on wall materials in ITER. Thus the Post–Jensen results have given a big contribution to the evaluation of the radiation effects. However recent progress in atomic physics is not included in them. Improvement of the calculations is of great importance to get a more exact quantitative estimates for the high Z impurity problems in the future.

An effort to calculate the molybdenum cooling rate as a function of T_e has been conducted intensively in a collaboration between LLNL, The Hebrew University (Jerusalem), The Johns Hopkins University and MIT [30]. Collisional radiative models for the X-ray, XUV, VUV and even visible line emission from Mo^{6+} to Mo^{39+} have been constructed. The data from the strong lines in those models (collision rates, Einstein coefficients, etc.) have been entered into the MIST code. Extensive calculations of dielectronic recombination and excitation auto-ionization have been performed for Mo^{33+} to Mo^{23+}. The results of those calculations have been put into the ionization balance

calculation performed by MIST. The EA rates for Mo^{6+} to Mo^{13+} done by Mitnik et al. [31] have also been put into the ionization balance calculation done by MIST. The results of the modified ionization balance calculation are seen in Fig. 7. The actual calculation of the EA and DR data will be published soon.

A preliminary results of the cooling-curve calculation suggests a possible shift of the curve to the lower temperature direction. This would give a considerable impact on the discussion on the cause of accumulation given in Section 2.1, where a flat T_e dependence is assumed in this region based on the Post–Jensen curve. [2]

2.4. Other remarks on core plasma issues

Influence of high Z impurities on other points, such as confinement improvement, thresholds of LH transition, contamination by low Z impurities such as oxygen or carbon are issues to be addressed now. For instance, the oxygen gettering/recycling property is quite different depending on materials. It might result in different behavior/concentration of oxygen with Mo and W walls/divertors.

Behavior of an H-mode plasma is under investigation in HT-6M tokamak in ASIPP/Hofei in China with and without a Mo limiter under boronized wall condition [32].

It is claimed that a higher hydrogen reflection coefficient of high Z wall cause deeper penetration of hydrogen atoms in the periphery, which results in loss of the ion momentum, a decrease in the radial electric field, and degradation of the confinement improvement [33].

Issues discussed in Section 2 are categorized as those of transport/atomic processes of high Z impurities in the core region. Although these are a bit outside the PSI research field, we must keep continuous attention to them.

3. Plasma surface interactions and behavior in edge plasmas

3.1. Origin of high Z impurities

In limiter tokamaks, the major origin of metal impurities are the limiter surfaces to which a plasma is attached [34]. This was confirmed in TEXTOR by inserting a small Mo test limiter into the plasma periphery.

In Alcator C-Mod, Mo I line radiation has been monitored during discharges, which are usually started with a limiter configuration and switched to a divertor configuration at several hundreds milliseconds after the ignition. In

---

[2] Added in proof: More recent revision of the analyses concludes that deviation of the results of ab initio calculation shows only a slight deviation from those by the Post–Jensen curve.
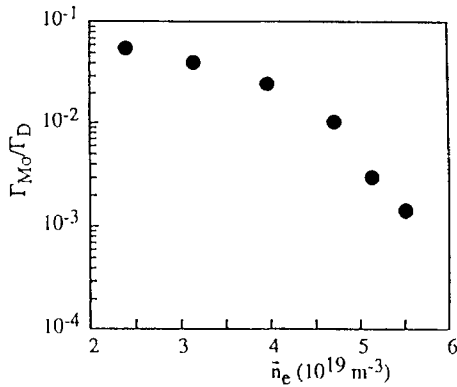
Fig. 10. Ratio of molybdenum flux Γ_{Mo} to deuterium flux Γ_D at the limiter surface of FTU [12].

the initial phase, Mo I lines from the inner wall, which is made of molybdenum and acting as a limiter, is dominant. After moving to a single null divertor configuration, the Mo I radiation zone is changed to the divertor region [35]. Because of the limits in spatial resolution, the local position has not yet been identified.

In OH discharges of FTU, the line radiation Mo I and $D\gamma$ at the poloidal Mo limiter was investigated for wide range of average plasma densities. Fluxes of Mo and deuterium were determined from the measured Mo I and $D\gamma$, and plotted in Fig. 10. It should be noted that, at $n_e > 6 \times 10^{19}/m^3$, the Mo I signals were reduced within the noise level of the detector. The author reported that the ratio of the flux can be interpreted as an effective sputtering yield of Mo by D^+ and self sputtering, and the physical sputtering is the only mechanism for impurity production [12–14].

In ASDEX Upgrade, erosion of tungsten markers by arcing is reported [9]. Arcing is frequent during NB heating, especially during transition from double-null to single-null configuration and during disruptions. For a plasma current larger than 1 MA, the arcing occurs frequently and it is critical in respect to erosion yield. In Ref. [9], the authors discussed a possible relation between the electric arc ignition and hot spots.

Arcing and/or disruptions could be one of the possible mechanisms of erosion, by which the life time of the limiter or divertor might be limited, if they would occur frequently. More systematic studies are necessary in tokamaks.

3.2. Enhanced sputtering with impurity ions

The impurity atom flux at the molybdenum limiter surface has been investigated as a function of the average electron density in TEXTOR. Fig. 11(a) shows the edge electron temperature and density measured by atomic He beam diagnostic at the mid-plane of $r = 46$ cm for an ohmically heated discharge [6]. The molybdenum limiter
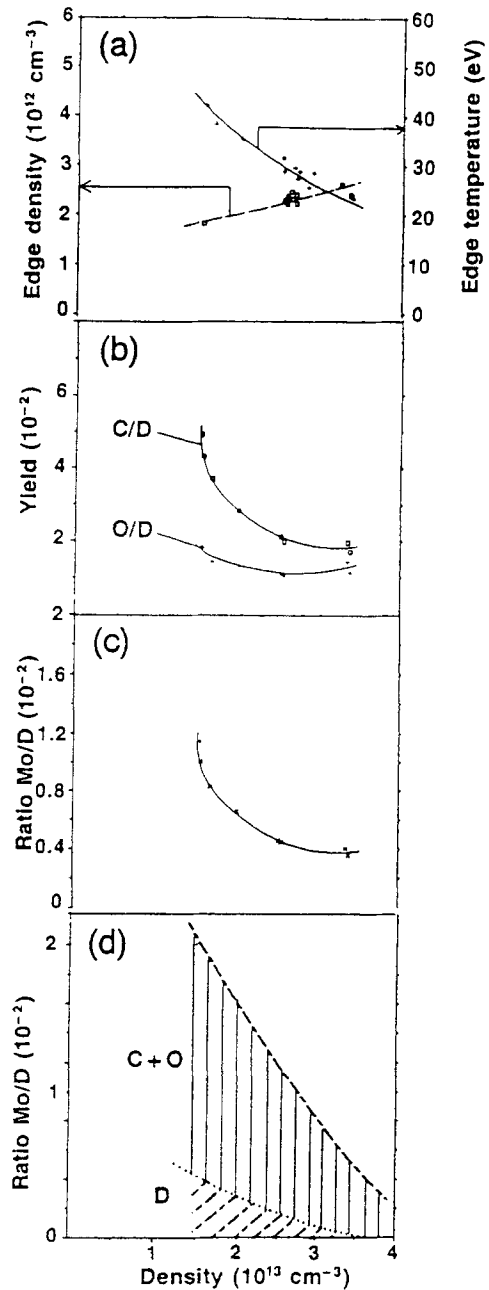

Fig. 11. Density dependence of edge fluxes at the Mo limiter surface in TEXTOR; (a) edge electron density and temperature at the last closed flux surface at the midplane, (b) C/D, O/D flux ratio, (c) Mo/D flux ratio, (d) contribution of Mo due to D ions' impact and due to C and O ions' impact estimated from measured C/D and O/D ratio in (b) [6].

was at $r = 44.5$ cm. The ratios of the emitted C and O to the D fluxes have been measured absolutely and plotted in Fig. 11(b). Absolute Mo fluxes at the limiter surface have been determined by spectroscopy of neutral Mo atoms.
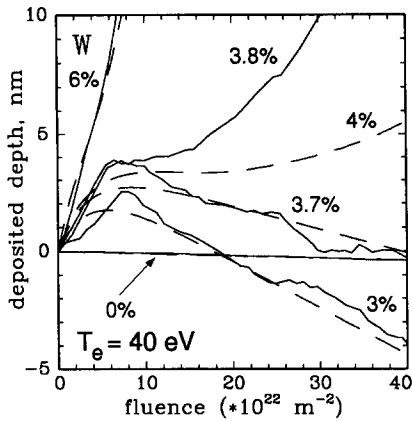
Fig. 12. Carbon deposition and erosion at the surface of a tungsten target as a function of fluence and carbon concentration in the plasma [39].

The combination of two Mo I lines at $\lambda = 414.36$ nm and 390.30 nm is utilized. The experimentally determined excitation cross-section is available [36] for the latter, whereas the former is relatively bright and unblended. The ratio of $I_{\mathrm{MoI}}/D_\alpha$ is plotted in Fig. 11(c). The values are in the range between $(0.4–1.2) \times 10^{-2}$. After careful analyses of the absolute and temperature dependences of this ratio, it turns out that Mo sputtering results predominantly from sputtering by impurity impact rather than by deuterium. This is demonstrated in Fig. 11(d). Coverage of the surface by carbon is estimated using data in Fig. 11(b) and taken into account in this analysis.

Contribution of low Z ion impact to tungsten sputtering has been also reported in a PISCES-B experiment [37]. Enhancement of the apparent sputtering yields are observed with impact of deuterium plasmas. This enhancement and the lowering of threshold temperature for sputtering are explained by taking the oxygen contribution into account.

Thus experimental evidences have been added for sputtering of high Z elements by the low Z impurities. This problem, together with the formation of protecting layer, is important to estimate high Z metal flux based on known plasma density and temperature in front of the surface.

Self-sputtering runaway has been one of the concerns listed in Ref. [1]. However it has not yet been experimentally identified for high Z metals.

3.3. Protection layers by low Z impurities

In plasma devices, wall surfaces facing to the plasma are always modified by impact of plasma particles and radiation, and not identical to the original surfaces any more. This influences the surface properties such as sputtering and hydrogen retention [38].

As mentioned briefly in the previous section, the coverage of carbon on Mo is estimated using a simple valance

equation, the measured flux ratio in Fig. 11(b) and sputtering data published in literature. It is 0.65 in this case. It is mentioned in Ref. [6] that this coverage reduces the erosion rate of molybdenum.

Sputtering of tungsten and carbon was analyzed under simultaneous bombardment by carbon and deuterium in Refs. [9,39]. A Monte Carlo program named TRIDYN was used in this calculation. A result of the TRIDYN calculation for a tungsten target is shown in Fig. 12 together with the results of a simplified approximation in an analytical model. The behavior is sensitively dependent on the fraction of carbon in the incident flux as seen in the figure. For a fraction above 3.7%, the tungsten surface is completely covered by carbon and no erosion occurs. The authors note an attention to highly non-linear change of the surface composition with an environment of multi-material configuration of plasma facing walls [9]. More detailed analyses are in progress [40].

3.4. Impact of low Z impurity injection

The reduction of the heat flux to limiter/divertor surfaces is a crucial issue to establish reasonable heat load on the target plates. Intensive studies on low Z impurity injection are performed in many tokamaks in order to
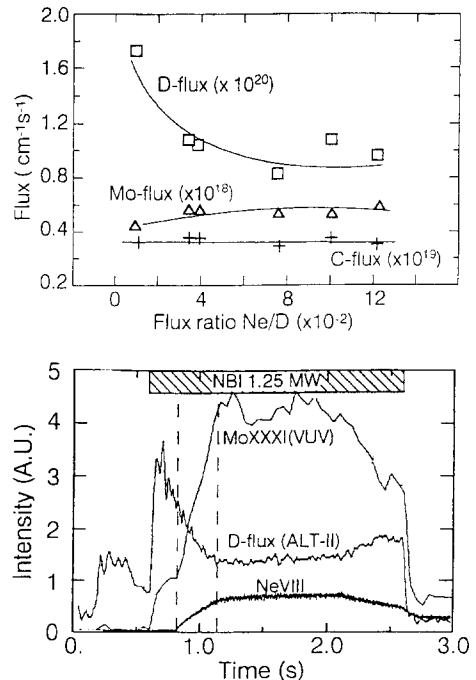

Fig. 13. (top) D-, Mo, C-fluxes on the Mo test limiter as a function of the flux ratio of Ne/D in TEXTOR Mo-limiter experiments [41]. The fluxes are integrated in the poloidal direction (unit: $cm^{-1}\ s^{-1}$). (bottom) Time evolution of the D-flux from the ALT-II limiter, a Mo XXXI line (17.7 nm), and a Ne VIII line. The line-averaged density is $3 \times 10^{19}/m^3$.

achieve this power reduction. Gas impurities such as neon, argon and nitrogen are used in these experiments.

Impact of neon injection upon high Z impurity behavior has been investigated in TEXTOR for ohmically and NB heated plasmas. Fig. 13(a) shows neutral fluxes at the molybdenum limiter plotted against the flux ratio of neon to deuterium [41], which is roughly proportional to injected amount of neon. No significant change in the Mo flux due to the neon injection is seen. This can be interpreted as a result that the effect of the edge temperature decrease by the injection on sputtering is compensated by the effect of the increase in the averaged charge and mass of ions which impact on the limiter surface. On the contrary, central radiation of Mo XXXI increases by a factor 4 compared with the intensity just before the injection, as seen in Fig. 13(b) [41]. This suggests that molybdenum accumulates with neon injection. Recent experiments on NB heated discharge with a tungsten limiter in TEXTOR shows remarkable effects of neon injection, where accumulation of

Fig. 15. Distribution of redeposited marker atoms in toroidal direction on the divertor plates of ASDEX Upgrade [45].

tungsten to the plasma axis and temperature collapse can be caused by neon cooling under certain conditions [42]. Some indications exist that this can be avoided with ICRF heating [19], but further studies are needed. The accumulation observed in these experiments can be understood by a neoclassical effect in ionic collisions where higher Z ions causes stronger inward flow of impurity ions.

Thus compatibility of high Z materials with the edge cooling is a new concern and has to be investigated more quantitatively.

3.5. Erosion, prompt re-deposition of sputtered atoms

Re-deposition is important from a viewpoint of reducing impurity contamination to the plasma and erosion rate of the surface. A careful experimental investigation on erosion and re-deposition processes was carried out in ASDEX Upgrade. Surface markers of silicon and tungsten on divertor tiles were exposed to 80 well defined plasma discharges. The profiles of the eroded and re-deposited materials were measured by ion beam analysis. Results have given us evidence of local deposition of sputtered tungsten ions named 'prompt re-deposition' due to the short ionization length and the relatively large gyro-radius [9,43–48].

Ionized W impurities return to the surface close to the emitted location within one gyro-motion and deposit because the magnetic field lines are almost parallel to the surface of divertor plates. The probability f of prompt redeposition is a function of a parameter p given as $f = \frac{1}{2}\{1 + \text{sig}(1-p)[1 + 4p^2/(1-p^2)^2]^{-1/2}\}$, where $p = \lambda_{\text{ion}}$ (ionization length)/ρ (gyro radius) [44]. A 3D Monte-Carlo code 'ERO' has been developed taking the gyro-motion effects into account [47]. A comparison between the analytical and the Monte-Carlo code calculations
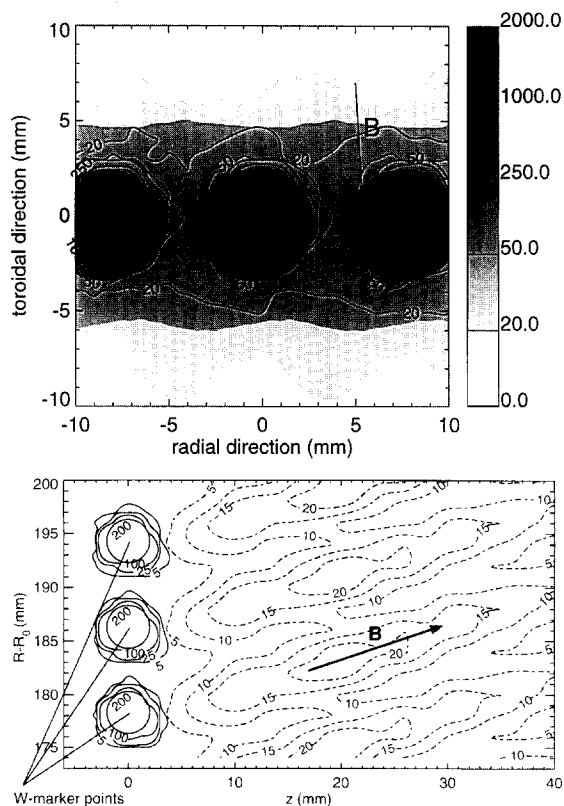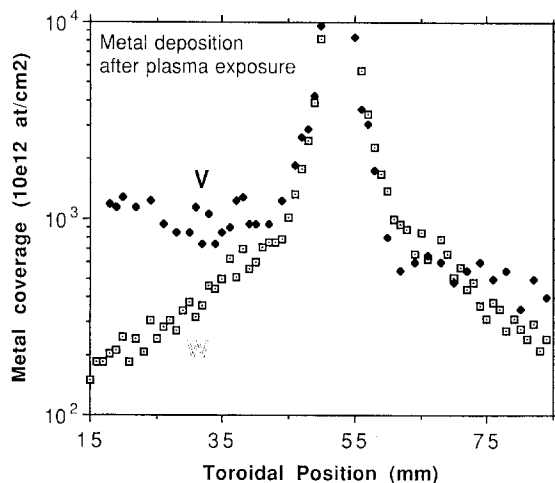

Fig. 14. Measured (top) and calculated (bottom) contour plot of the W distribution after exposure of the original marker spots (solid circles in bottom) to about 80 divertor discharges in ASDEX Upgrade. The levels correspond to the thickness of the redeposited W in nm. Without taking into account the gyration (prompt redeposition) effects, the measured results does not agree with the calculated distribution by the ERO code (as indicated by dashed contour in the figure) [43].

was carried out and a good agreement was obtained [9,44]. The ERO code was applied to the experimental condition in ASDEX Upgrade. Fig. 14 shows an experimentally observed profile (top), and the calculated results (bottom) with and without the gyro-motion effects. Remarkable difference can be seen between two calculated results. The measured deposition pattern agrees much better with the calculated result with the gyro-motion. Thus the importance of the gyro-motion effect was demonstrated.

The erosion and deposition pattern was compared between tungsten, vanadium and silicon in ASDEX Upgrade [45]. Silicon atoms spreaded toroidally over many cm and vanadium atoms showed migration predominantly downstream along the field lines. On the contrary very local deposition was observed for tungsten close to the original marker spot. The decay length is less than 10 mm as seen in Fig. 15. A similar result was obtained in DiMES experiments in DIII-D [49–51]. This was successfully modeled by the WBC Monte Carlo code [52].

TEXTOR 2D spectroscopic patterns of Mo I and W I

Fig. 17. Fraction of prompt redeposition calculated with ERO including E-field (A), singly charged W (B), all effects (C) [9].
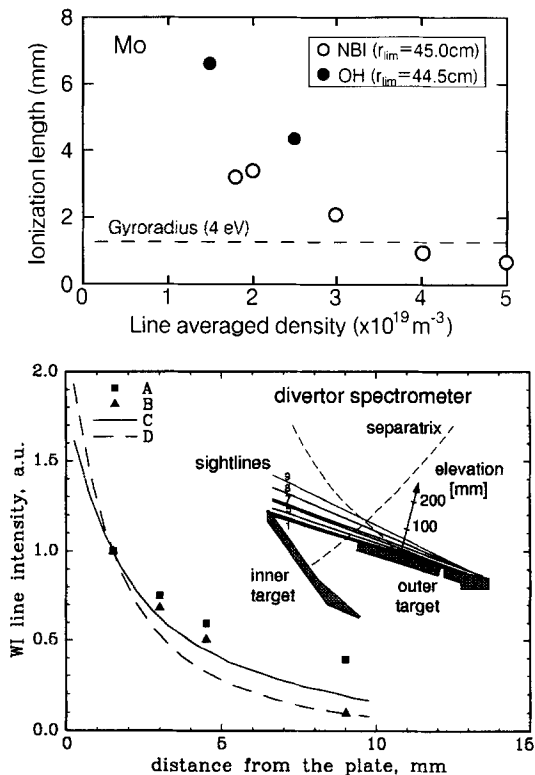

Fig. 16. Ionization length of neutral Mo atoms(top) determined by the decay length of Mo I intensity near the Mo test limiter in TEXTOR for OH plasmas (closed circle) and NB plasmas (open circle). The gyro-radius of Mo^+ is about 1.3 mm [41]. Measured WI radiation profile in ASDEX Upgrade (bottom) for two different line averaged densities (A) 1.7×10^{19} m^{-3} and (B) 2.0×10^{19} m^{-3}. Two lines are obtained by ERO for divertor density of (C) 1.0×10^{18} m^{-3} and (D) 3.0×10^{18} m^{-3} [9].
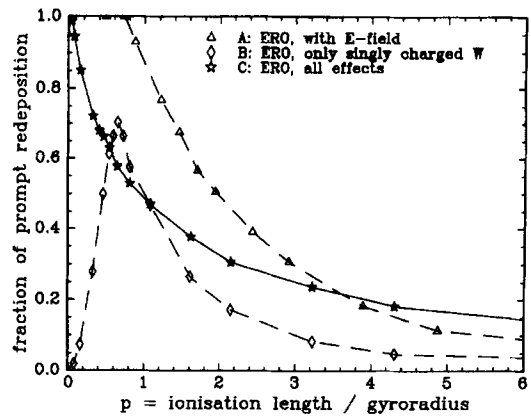
show that their radial penetration depth decreases down to less than 1 mm at high local plasma densities [41,54]. Fig. 16 (top) shows the measured ionization length in front of the Mo limiter surface. It decreases down to less than 1 mm for a line-averaged density of 5×10^{19} m^{-3}, which is well shorter than gyro-radius of Mo^+ ions with 4 eV [41]. An even stronger effect is reported from ASDEX Upgrade tungsten experiment and shown in Fig. 16 (bottom) [9,55]. Comparison between WI profiles and calculations using the ERO code have been tried for both in TEXTOR and ASDEX studies. In Fig. 16 (bottom), the results by ERO are also shown for the ASDEX case.

It is already mentioned that the computational codes 'ERO' [43] and 'WBC' [52] are quite powerful to reproduce the experimental results above described. The WBC code computes the sub-gyro-orbit motion of an individual sputtered particle, including the Lorentz force motion, and charge changing and velocity changing collisions with the plasma. Multiple ionization processes, frictional and thermal forces, etc. are thus rigorously taken into account. In principle, all processes are includeable in a Monte Carlo code such as WBC, but longer computational time may be needed to minimize variance. Together with the REDEP gyro-orbit-averaged deterministic code, and the BPH1 kinetic sheath [53] code, prediction has been given for very high local redeposition of sputtered tungsten, including ionization in the millimeter-scale oblique-incidence tokamak sheath, and subsequent return to the surface via the strong electric field acceleration. The ERO code contains many of the features of WBC and, has already been mentioned, has been applied to the ASDEX studies. The analytical model describing the protection effects discussed in Section 3.3. is included into the ERO code. In Fig. 17, the fraction of prompt re-deposition is plotted as a function of the parameter p, in which a contribution of singly charged tungsten ions is indicated [9].

A dynamic simulation code is under development to apply sputter and deposition processes on tungsten sur-

faces. The composition change with time can be calculated taking into account the trajectories of sputtered ions close to the surface [56].

All the results in this sub-section show that the prompt re-deposition, which is prominent for high Z ions, gives a very promising effect to prevent impurity penetration into the SOL and to reduce the erosion significantly.

3.6. Transport of impurities in divertor and SOL

It is expected in future devices that only a part of strong plasma–surface interaction will be with erosion-resistant materials. Most of the plasma facing wall is not necessarily made of such materials. In that case, some fraction of divertor/limiter material ions could escape to the wall during the travel in SOL, and do not reenter to the SOL for a long period even when the charge exchange flux contributes to re-emit deposited materials on the wall. If this is the case, the scrape off layer might have some shielding effect on the flux from limiter/divertor to core plasmas. The analysis of this effect is also necessary to get a comprehensive picture of the high Z impurity migration.

A deposition probe was utilized in TEXTOR to get information for impurity transport in the SOL. The probe was located 150° away from the Mo test limiter in toroidal direction. The flux of molybdenum atoms transported from the test limiter to the probe decreases with average plasma density [6]. It has been found that the ratio of the deposition density to sputtered flux is much smaller with W limiter than with Mo limiter [57]. This indicates that less tungsten atoms are transported to the location of the surface probe through the scrape off layer. However, less deposition could be explained from the lower sputtering yield and the higher prompt re-deposition rate, only. It is hard to discriminate the SOL transport and the local effects by a measurement at one location.

3.7. Hydrogen isotope retention

Deuterium retention was measured and compared among W, Mo, V, C, Be in D III-D. Small coupons of these metals were deposited onto the surface of DiMES samples [51]. The nominal thickness of the films was 100 nm. Retention of deuterium in the samples was mapped by nuclear reaction with a 700 keV ^{3}He beam. The samples were exposed to ELM-free quiescent H-mode deuterium plasmas. Integrated exposure time was 14 s. The sample arrangements and results are shown in Fig. 18. It is clearly seen that surface densities of D atoms on Mo and W were smaller by factors 3 to 5 compared to Be and C. The authors speculate that this observed small aerial density is due to the fast diffusion of D in body centered cubic metals above room temperature, so that the deuterium can migrate to the external surface and leave.

Co-deposition of deuterium with tungsten, carbon and beryllium was investigated by Mayer et al. No co-deposi-
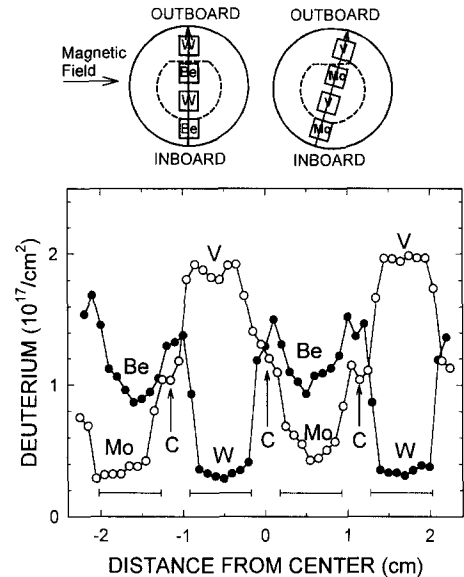

Fig. 18. Deuterium retention obtained in D III-D with the DiMES probe. The arrangements of the coupons are shown for W and Be (top, left, sample No. 71), and for V and Mo (top, right, sample No. 70). The horizontal axis is the distance from the center in radial direction [51].

tion of deuterium with tungsten was observed in contrast to the other two materials [58].

Another investigation is reported on thermal desorption of plasma sprayed tungsten coatings by a Garching group [59]. Samples were implanted with 300 eV D^{3+} at room temperature with a fluence varying from 1×10^{17} D/cm^2 to 1×10^{18} D/cm^2. The amount of retained deuterium was obtained by integrating the spectra of thermal desorption. It is found that the retained amount is proportional to the porosity of the samples. The absolute amount is of the same order of magnitude as in graphite. Deuterium retention in five types of tungsten samples has been reported in Ref. [60]. It is shown that D is retained far beyond the implanted zone. It is worthwhile to draw the readers' attention to the papers in this conference which contribute to give us present understanding on this issue [61–65].

It should be also mentioned here that the retention could change depending on surface composition as discussed in Section 3.3, surface temperature, microscopic geometry on the top surface etc. Therefore, much more data must be accumulated from now on for various conditions and comprehensive analyses will be necessary.

3.8. Particle and energy reflection

The impact of particle and energy reflection, especially energy reflection is one of the interesting issues [1] and discussed in TEXTOR experiments [54,66]. The heat deposition to a W limiter was slightly smaller than the one to a

Mo limiter [66]. However no clear difference was observed between Mo and C limiters so far. Thus whether energy deposition really differs depending on the limiter material is still unclear within the experimental accuracy. It should be noted that this topic has not yet examined in detail.

4. Material studies and development

4.1. Postmortem analyses of exposed surfaces

Molten layers and recrystallization were found on a Mo limiter after exposure to TEXTOR plasmas, in which maximum heat load has been estimated as 20 MW/m^2. The cracks were located just above a hole for a thermocouple [66,67].

During the operation, large enhancement of the Mo I line was observed for two high power heated discharges. It is likely that the melting occurred in these two shots. In Fig. 19, the time behavior of Mo I is plotted together with other parameters [66]. It is worth to note that, in spite of the large increase in Mo I radiation, no increase in molybdenum at the plasma center (Mo XXXI) has been observed. This suggests that vaporization at the limiter surface does not affect plasma behavior. It was reported that severe melting was found in Mo limiters in TRIAM-1M tokamak after use in long time discharges extending over 1 h [68]. It may be possible that evaporated Mo cannot penetrate into the plasma due to its extremely low energy. Damage and recrystallization are reported for TiC coated molybdenum divertor tiles in JT-60, too [69].

It is worth to note that, in the experiments of long time discharges in TRIAM-1M, samples exposed to charge exchange neutral flux show remarkable numbers of dislocation at the top surface [70]. The authors claim some influence of this damage on plasma surface interactions, such as tritium retention in the wall. Post mortem analysis of Mo and TZM limiters of FTU is presented at this conference [71].

4.2. Research and development of tungsten coated graphite for application to ASDEX Upgrade

In ASDEX Upgrade, an experiment with a full-toroidal tungsten divertor is going on [72]. Careful considerations and R&D efforts have been conducted to find a good tungsten material for this experiment [73–75]. One possibility was to utilize the tungsten–lanthanum alloy, WLO (W + 1 wt% La$_2$O$_3$), being a recent development and recommended by Metalwerk Plansee AG. This material is one of the candidates for ITER divertor and an intensive work is under way in KFA Jülich [76]. In the ASDEX experiment, a tungsten coated graphite is finally chosen. There are a number of reasons why the coated tungsten was chosen instead of bulk tungsten. One of the main
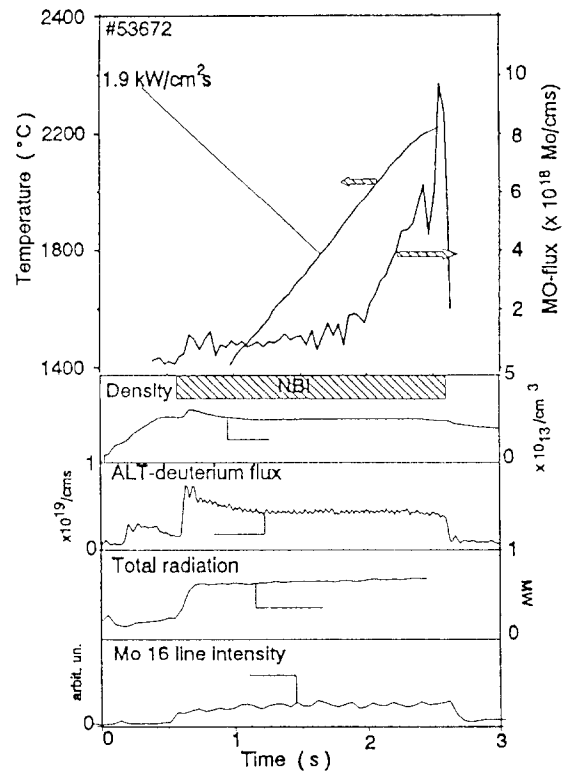
Fig. 19. Time behavior of plasma parameters for the particular shot where the molybdenum limiter is subjected to surface melting in TEXTOR, as seen in the increase in Mo I line [66].

reasons was high forces due to eddy currents during disruptions possible in the bulk tungsten material because of the high electric conductivity [73].

A series of high heat load test were carried out for four kinds of tungsten coated graphite tiles [74,75]. Three of them were with tungsten layers of 150–550 μm thickness coated by plasma spray (PS) and the other one was with layers of 20–100 μm thickness coated by physical vapor deposition (PVD). Heat load tests were performed at the electron beam facility JUDITH (Jülich Divertor Test Experiment/Hot Cells), and at the hydrogen beam test stand MARION (Material Research Ion Beam Facility) at the Research Center (KFA) Jülich.

While the PVD coatings showed failure at a heat load below 14 MW/m^2, two of the three PS coatings were found to tolerate up to 16 MW/m^2. Under cyclic heat load of 10 MW/m^2 and 2 s pulse length, no disabling damages were found for the PS coatings. The PVD coatings failed by extensive crack formation under the same condition. These results indicate that the PS coatings are more resistant to high heat load, which can be interpreted by its crack-arresting mechanism due to higher porosity. One of the PS coatings was finally chosen for the full toroidal divertor experiment in ASDEX Upgrade.

4.3. Material developments in the future

Near term and long term requirements should be separately approached. In the near term applications, influence of DT neutron irradiation would be less important compared to future reactors with high neutron fluence. For the near term application, tungsten coated carbon could be convenient because carbon tiles could be easily replaced without big change in heat transfer property to cooling channels.

In the long term application, the following issues are relatively important.

(i) Tolerance to high neutron fluence for reduction of number of replacements during a reactor life.

(ii) Combinations with low activation materials are desirable, important or critical.

(iii) A new approach from coolant side is as important as an approach from plasma side, which has long been taken in plasma experimental devices up to now because of the emphasis on achieving high performance plasmas. For instance, a material with which we can fabricate a cooling channel should be chosen at first, then some transition to a material which is favorable for plasmas could be considered. Most desirable is that the coolant channel itself can be directly exposed to the plasma edge, which could be possible if we do not have a concern about local heat concentration or disruptions.

Another important requirement is 'less-activation' under D–T neutron irradiation. This will be one of the most critical problems because PFC such as divertor target plates will be replaced several times during a life time of future D–T reactors. It means that a considerable amount of waste must be safely stored. It would be desirable to utilize materials without long-life activation under the D–T neutron irradiation.

As an example, tantalum could be a good candidate because of the following characteristics.

– Cooling tube already commercially available.

– High resistivity to cooling water.

– Relatively high ductility and good in bonding to other metals such as austenitic stainless steel.

– No long life products under DT neutron irradiation, namely, a low activation material.

– Resistant to erosion by plasma impact due to high Z and high mass number similar to W.

A large problem is the tritium inventory due to its exothermic characteristics with hydrogen isotope absorption. This might be overcome by making a protecting layer of tungsten.

The most recent review for thermo-mechanical and chemical characteristics of various high Z metals are given in Ref. [77]. It should be mentioned that some other activities on the development are in progress in the US and Japan, which could not be reviewed this time. Another review should be given in the near future about the high Z materials from material-development side.

5. Discussion

From a practical point of view, radiation loss power and central impurity density is one of the big issues to be investigated as a function of various conditions of plasma parameters and environments. As shown in previous sections, many factors in the core and PSI give impacts to this relation. A simplified overall picture in divertor configuration can be given as follows.

In a steady state, the net impurity influx to the divertor plasma $\Delta\Phi = \Phi_{\text{sputt}} - \Phi_{\text{redep}}$ is equal to $n_{\text{div}} v_{\text{drift}}$ at the ionization front close to the surface, where n_{div} is the impurity density in the divertor plasma, Φ_{sputt} the flux toward the divertor plasma due to sputtering, Φ_{redep} the redeposited flux to the surface, and v_{drift} the drift velocity of the impurity ions along the field lines. If one uses a penetration factor γ_{penet} defined as $1 - (\Phi_{\text{redep}}/\Phi_{\text{sputt}})$, $\Delta\Phi$ is written as $\gamma_{\text{penet}}\Phi_{\text{sputt}}$. A loss flux Φ_{loss} to the wall gives another shielding factor γ_{sol} to the influx through the LCFS and determines the average impurity density n_{sol} in the scrape-off layer as $n_{\text{sol}} \approx \gamma_{\text{sol}}\gamma_{\text{penet}}\Phi_{\text{sputt}}/v_{\text{drift}}$. In the core region, the density profile can be written as $n(r) = n_0 \exp[-C_v r^2/a^2]$ if the inward velocity is assumed to be $v_{\text{in}}(r) = -rv_{\text{ain}}/a$ [78], where n_0 is the impurity density at the plasma axis, a a minor radius of the core, C_v the peaking factor defined as $C_v = av_{\text{ain}}/2D$ with diffusion constant D and inward velocity of v_{ain} at the boundary. The boundary condition of the core plasma is $n(a) = n_{\text{sol}}$. Then the overall expression is

$$n_0 \approx \gamma_{\text{sol}}\gamma_{\text{penet}}(\Phi_{\text{sputt}}/v_{\text{drift}})\exp[C_v].$$

Thus the central density n_0 is given as a product of several factors above described. The sputtered flux can be determined with the incident ion fluxes, surface coverage by other impurities, edge plasma parameters etc., to which discussions in Sections 3.1, 3.2, 3.3 and 3.4 are related. As discussed in Section 3.5, γ_{penet} is determined by redeposition of emitted impurities. The other factor γ_{sol} is determined by diffusion across field lines in the SOL discussed in Section 3.6. The profile in the core plasma is strongly dependent on the inward velocity divided by the diffusion constant given as C_v, which is discussed in Section 2.1, partly in Section 3.4 and closely coupled with the discussion in Section 2.3. Thus the question can be disintegrated to the questions to get these 4 factors in the above equation including Φ_{sputt}. This simplification may possibly help us to have easier scope of the impurity concentration, and therefore the radiation loss power in the core.

The analysis in Section 3.3 indicates that low Z layers are certainly formed on high Z metal surfaces if they are surrounded by other materials such as carbon tiles. This layers would be acting as the protecting layer for high Z surfaces. If the protecting layer could be provided intentionally in a controlled manner, it would help to some extent to reduce the penetration of high Z impurity atoms

into the plasma and to mitigate erosion of the surface. As an example, conventional in-situ boronization is one possible way to realize this intentional protecting layer. Or another possibility is short time application of real time boronization [79,80] during a long time operation of the main discharge with magnetic field, which could make the coating preferentially on the target surface of severest interaction with the discharge plasma. This can be done by putting some reactive gas into the plasma. If this technique is established, merit of low Z coating for core plasma performance can be combined with the low erosion rate of high Z target surface. Most of the first wall can be originally composed with medium Z, low activating metals such as vanadium. Pre-coating of low Z thin films might be sufficient to prevent direct exposure to the plasma. Immigration of materials between target plates and other walls is not necessarily symmetric. Then it is necessary to study the gross immigration behavior of the materials between the divertor and the other part of PFC.

Recently the boronization have been applied both to ASDEX Upgrade with a full tungsten divertor, and to Alcator C-Mod with a full molybdenum divertor. Although the first motivation in these experiments might not be the protective layer but other profits of boronization such as high performance of core plasmas and/or wide range in the operation field, it would be worthwhile to address the above described issue there.

Of cause there is a possibility that the protective coating does not work at all, or does just partly work in which case the part of the severest interaction cannot have sufficient coverage of low Z coated layer. Then systematic studies without low Z coating are still necessary and important.

6. Conclusions

Conclusions which have relative importance in future studies are listed as follows.

(1) In critical conditions, high Z impurity causes strong radiation loss from the plasma center, which results in reduction in $T_e(0)$ and flattening in $T_e(r)$.

(2) The enhanced radiation is attributed to a transport phenomenon, namely the accumulation of high Z impurity toward the plasma axis.

(3) This strong accumulation of high Z impurities occurs only in a limited number of cases, such as relatively high density OH discharges (TEXTOR), some NB heated H-mode (ASDEX Upgrade), or neon-injected (TEXTOR) discharges.

(4) No accumulation has been found in any case of ICRF heated discharges with a sufficient heating power, which cannot necessarily be attributed to direct coupling between rf and impurity ions.

(5) From these observations, one can say that a wide operation area could be expected without serious accumu-

lation. But compatibility of high Z materials with the edge cooling by low Z gas impurities is a concern and has to be investigated more quantitatively.

(6) A systematic study on Mo radiation in Alcator C-Mod indicates the importance of the excitation auto-ionization (EA) process of multiple-charged Mo ions. An effort has been made to reproduce the radiation-cooling rate by Mo ions versus temperature curve (corresponding to the Post–Jensen calculation) based on the modern calculation of atomic processes and experimental evidences in Alcator C-Mod.

(7) Prompt re-deposition has been experimentally confirmed. It helps much either to avoid the impurity penetration into the divertor plasmas, or to mitigate the surface erosion. It has been demonstrated in ASDEX Upgrade and D III-D that the erosion rate of tungsten is much smaller than that of medium Z materials such as silicon, vanadium etc.

(8) Protecting layers by low Z impurities on high Z surfaces can play a role to reduce sputtering of high Z metals. Intentional combination of low Z coating, such as boronization, with high Z plasma facing components is an attractive concept. This has been addressed preliminary in the full toroidal tungsten divertor experiment in ASDEX Upgrade and the molybdenum divertor experiment in Alcator C-Mod.

(9) Deuterium retention measured with a tungsten coupon in D III-D does not agree with those in plasma-sprayed W coated graphite samples adopted in ASDEX Upgrade. Co-deposition of deuterium with tungsten does not occur.

(10) Development and evaluation of high Z materials has been started aiming at a short-term and a long-term target. In the short-term studies, tungsten coated carbon materials have been selected and are actually tested in a KFA Jülich-IPP Garching collaboration. A plasma-sprayed tungsten on isotropic graphite is successfully applied in ASDEX Upgrade. In long-term studies, compatibility with the coolant and low activation by D–T neutron irradiation should be considered as important criteria.

It should be stressed once more that most of the above listed conclusions are still tentative and a lot of works have to be done in future before getting final conclusions and approaching the goal of this study. Because of the limitation in space, the review of material development was impossible in this paper. Only limited space was allocated to this issue, for which another review is necessary in the near future.

Acknowledgements

References

[1] T. Tanabe, N. Noda and H. Nakamura, J. Nucl. Mater. 196–198 (1992) 11.

[2] G. Janeschitz, K. Borras et al., J. Nucl. Mater. 220–222 (1995) 73.

[3] R.J. Hawryluk et al., Nucl. Fusion 19 (1979) 1307.

[4] V. Arunasalam et al., Proc. 8th EPS. 1977, Prague Vol. 2, p. 17.

[5] H. Nakamura et al., Nucl. Fusion 28 (1988) 43.

[6] V. Philipps, T. Tanabe, Y. Ueda et al., Nucl. Fusion 34 (1994) 1417.

[7] V. Philipps, A. Pospieszczyk et al., in: Plasma Physics and Controlled Fusion Research 1994 (IAEA, Vienna, 1995) II, p. 149 (15th IAEA Conf. in Sevilla, 1994, IAEA-CN60/A2/4-p-19).

[8] V. Philipps, M. Tokar, A. Pospieszcyk et al., in: Proc. 22nd EPS (1995), Bournemouth, Vol. 19C, Part II, p. 321.

[9] D. Naujoks, K. Asmussen et al., Nucl. Fusion 36 (1996) 671.

[10] K. Asmussen, PhD thesis, IPP-Report 10/2 (1996), Max-Planck-Institut für Plasmaphysik, Garching.

[11] R. Neu, K. Asmussen et al., in Proc. of 22nd EPS (1995), Bournemouth. Vol. 19C, Part I, p. 65.

[12] M.L. Apicella et al., to be published in Nucl. Fusion.

[13] F. Alladio et al., Plasma Phys. Control. Fusion 36 (1994) B253.

[14] F. Alladio et al., Proceedings of the International Conference on Plasma Physics (ICPP 1994) Foz Do Iguacu, Brazil, p. 158.

[15] M.Z. Tokar, T. Balemans, V. Philipps et al., Plasma Phys. Controlled Fusion 37 (1995) A241.

[16] R.V. Jensen, D.E. Post et al., Nucl. Fusion 17 (1977) 1187.

[17] D.E. Post, R.V. Jensen et al., At. Data Nucl. Data Tables 20 (1977) 397.

[18] R. Koch, A.M. Messiaen, J. Ongena et al., Fusion Eng. Design 26 (1995) 103.

[19] G. van Oost, A.M. Messiaen, V. Philipps, M. Wada et al., in: Proc. 21st EPS, 1994, Montpellier, Vol. 18B, Part II, p. 1020.

[20] G. van Oost, A.M. Messiaen, V. Philipps et al., in: Proc. 22nd EPS, 1995, Bournemouth, Vol. 19C, Part III, p. 345.

[21] J.E. Rice, J.L. Terry, K.B. Fournier et al., J. Phys. B 29 (1996) 2191.

[22] M.A. Graf et al., Rev. Sci. Instrum. 66 (1995) 636.

[23] B. Lipschultz, J. Goetz, B. LaBombard et al., J. Nucl. Mater. 220–222 (1995) 50.

[24] C. Kurz, B. Lipschultz, G. McCracken et al., J. Nucl. Mater. 220–222 (1995) 963.

[25] S. Itoh, N. Hiraki et al., Plasma Physics and Controlled Nuclear Fusion Research 1990, Vol. 1 (IAEA, Vienna, 1991) p. 733.

[26] J.E. Rice, F. Bombarda, M.A. Graf et al., Rev. Sci. Instrum. 66 (1995) 752.

[27] J.E. Rice, K.B. Fournier, M.A. Graf et al., Phys. Rev. A 51 (1995) 3551.

[28] R.A. Hulse, Nucl. Tech./Fus. 3 (1983) 259.

[29] K.B. Fournier et al., Phys. Rev. A, submitted.

[30] J.E. Rice and K.B. Fournier, private communication.

[31] D. Mitnic, P. Mandelbaum et al., Phys. Rev. A 50 (1994) 4911.

[32] J. Li et al., these Proceedings, p. 878.

[33] K. Itoh and S.-I. Itoh, NIFS-287, 1994, National Institute for Fusion Science.

[34] N. Noda, T. Watari, K. Toi et al., J. Nucl. Mater. 128&129 (1984) 304.

[35] K. Kondo, private communication.

[36] I.I. Sobelmann et al., in Excitation of Atomic and Broadening of Spectral Lines, Spring Series of in Chemical Physics, Vol. 7 (Springer, Berlin, 1981) 12217.

[37] Y. Hirooka, M. Bourham et al., J. Nucl. Mater. 196–198 (1992) 149.

[38] R. Behrisch, M. Mayer and C. García-Rosales, J. Nucl. Mater. 233—237 (1996) 673.

[39] D. Naujoks and W. Eckstein, J. Nucl. Mater. 220–222 (1995) 993.

[40] D. Naujoks and W. Eckstein, J. Nucl. Mater. 230 (1996) 93.

[41] Y. Ueda, T. Tanabe, V. Philipps et al., J. Nucl. Mater. 220–222 (1995) 240.

[42] V. Philipps, K. Ohya, T. Ohgo et al., private communication.

[43] D. Naujoks, J. Roth et al., J. Nucl. Mater. 210 (1994) 43.

[44] G. Fussmann et al., in: Plasma Physics and Controlled Fusion Research 1994 (IAEA, Vienna, 1995) II, p. 143 (15th IAEA Conf. in Sevilla (1994), IAEA-CN-60/A2/4-p-18).

[45] J. Roth, D. Naujoks, K. Krieger et al., J. Nucl. Mater. 220–222 (1995) 231.

[46] D. Naujoks and R. Behrisch, J. Nucl. Mater. 220–222 (1995) 227.

[47] D. Naujoks and R. Behrisch, in: Proc. 19th European Conference, Innsbruck, 1992, Vol. 16C II, p. 843.

[48] D. Naujoks, R. Behrisch, J.P. Coad et al., Nucl. Fusion 33 (1993) 581.

[49] R. Bastasz, W.R. Wampler et al., J. Nucl. Mater. 220–222 (1995) 310.

[50] T.Q. Hua and J.N. Brooks, J. Nucl. Mat. 220–222 (1995) 342.

[51] W.R. Wampler et al., J. Nucl. Mater. 233–237 (1996) 791.

[52] J.N. Brooks, Phys. Fluids B2 (1990) 1858.

[53] T.Q. Hua and J.N. Brooks, Phys. Plasmas 11 (1994) 3607.

[54] M. Wada et al., these Procedings, p. 799.

[55] A.R. Field et al., J. Nucl. Mater. 220–222 (1995) 553.

[56] J. Kawakita and K. Ohya, J. Appl. Phys. 35 (1996) L345.

[57] M. Rubel, B. Emmoth et al., private communication.

[58] M. Mayer, R. Behrisch et al., J. Nucl. Mater. 230 (1996) 67.

[59] C. Garcia-Rosales, P. Franzen et al., J. Nucl. Mater. 233–237 (1996) 803.

[60] V.Kh. Alimov and B.M.U. Scherzer, J. Nucl. Mater. 240 (1996) 75.

[61] A.P. Zakharov, A.E. Gorodetsky et al., these Proceedings, p. 52.

[62] Y. Yamauchi, T. Hino et al., these Proceedings, p. 1016.

[63] A.A. Haasz and J.W. Davis, these Proceedings, p. 1076.

[64] P. Franzen, C. Garcia-Rosales et al., these Proceedings, p. 1082.

[65] W. Wang, V.Kh. Alimov, B.M.U. Scherzer and J. Roth, these Proceedings, p. 1087.

[66] T. Tanabe, Y. Ueda, V. Philipps et al., Fusion Eng. Design 28 (1995) 13.

[67] T. Tanabe, V. Philipps, Y. Ueda et al., J. Nucl. Mater. 212–215 (1994) 1370.

[68] N. Yoshida, K. Tokunaga et al., J. Nucl. Mater. 196–198 (1992) 415.

[69] N. Yoshida, T. Kato et al., J. Nucl. Mater. 220–222 (1994) 371.

[70] T. Muroga, R. Sakamoto et al., J. Nucl. Mater. 196–198 (1992) 1013.

[71] G. Maddaluno et al., these Proceedings, p. 908.

[72] R. Neu et al., these Proceedings, p. 678.

[73] H.-S. Bosch, D. Coster, S. Deschka et al., IPP Report 1/281(1994), Max-Planck-Institut für Plasmaphysik, Garching.

[74] C. Garcia-Rosales, S. Deschka et al., Fusion Technol., to be published.

[75] S. Deschka, C. Garcia-Rosales et al., J. Nucl. Mater. 233-237 (1996) 645.

[76] J. Linke et al., private communication.

[77] T. Tanabe, in: 'Atomic and Plasma–Material Interaction Data for Fusion', Supplement of Nuclear Fusion Vol. 5 (IAEA, Vienna, 1994) p. 129.

[78] K. Ida, R.J. Fonck et al., Nucl. Fusion 29 (1989) 231.

[79] H.G. Esser, J. Winter et al., J. Nucl. Mater. 196–198 (1992) 231.

[80] A. Sagara et al., these Proceedings, p. 972.